AFRL-PR-WP-TP-2006-272

AN EXPERIMENTAL INVESTIGATION OF LOW-PRESSURE TURBINE BLADE SUCTION SURFACE STRESSES USING S3F (PREPRINT)

Mark McQuilling, Mitch Wolff, Sergey Fonov, Jim Crafton, and Rolf Sondergaard

OCTOBER 2006

STINFO COPY

PROPULSION DIRECTORATE
AIR FORCE MATERIEL COMMAND
AIR FORCE RESEARCH LABORATORY
WRIGHT-PATTERSON AIR FORCE BASE, OH 45433-7251

REPORT DOCUMENTATION PAGE

Form Approved
OMB No. 0704-0188

The public reporting burden for this collection of information is estimated to average 1 hour per response, including the time for reviewing instructions, searching existing data sources, searching existing data sources, gathering and maintaining the data needed, and completing and reviewing the collection of information. Send comments regarding this burden estimate or any other aspect of this collection of information, including suggestions for reducing this burden, to Department of Defense, Washington Headquarters Services, Directorate for Information Operations and Reports (0704-0188), 1215 Jefferson Davis Highway, Suite 1204, Arlington, VA 22202-4302. Respondents should be aware that notwithstanding any other provision of law, no person shall be subject to any penalty for failing to comply with a collection of information if it does not display a currently valid OMB control number. **PLEASE DO NOT RETURN YOUR FORM TO THE ABOVE ADDRESS.**

1. REPORT DATE *(DD-MM-YY)*	2. REPORT TYPE	3. DATES COVERED *(From - To)*
October 2006	Journal Article Preprint	07/01/2006 – 10/04/2006

4. TITLE AND SUBTITLE

AN EXPERIMENTAL INVESTIGATION OF LOW-PRESSURE TURBINE BLADE SUCTION SURFACE STRESSES USING S3F (PREPRINT)

5a. CONTRACT NUMBER
In-house

5b. GRANT NUMBER

5c. PROGRAM ELEMENT NUMBER
61102F

6. AUTHOR(S)

Mark McQuilling and Rolf Sondergaard (AFRL/PRTT)
Mitch Wolff (Wright State University)
Sergey Fonov and Jim Crafton (Innovative Scientific Solutions, Inc.)

5d. PROJECT NUMBER
2307

5e. TASK NUMBER
NP

5f. WORK UNIT NUMBER
02

7. PERFORMING ORGANIZATION NAME(S) AND ADDRESS(ES)

Turbine Branch (AFRL/PRTT)
Turbine Engine Division
Propulsion Directorate
Air Force Research Laboratory
Air Force Materiel Command
Wright-Patterson Air Force Base, OH 45433-7251

Wright State University
Mechanical and Materials Engineering
3640 Colonel Glenn Hwy.
Dayton, OH 45435

Innovative Scientific Solutions, Inc.
2766 Indian Ripple Road
Dayton, OH 45440

8. PERFORMING ORGANIZATION REPORT NUMBER

AFRL-PR-WP-TP-2006-272

9. SPONSORING/MONITORING AGENCY NAME(S) AND ADDRESS(ES)

Propulsion Directorate
Air Force Research Laboratory
Air Force Materiel Command
Wright-Patterson AFB, OH 45433-7251

10. SPONSORING/MONITORING AGENCY ACRONYM(S)
AFRL-PR-WP

11. SPONSORING/MONITORING AGENCY REPORT NUMBER(S)
AFRL-PR-WP-TP-2006-272

12. DISTRIBUTION/AVAILABILITY STATEMENT
Approved for public release; distribution is unlimited.

13. SUPPLEMENTARY NOTES
Journal article submitted to Experiments in Fluids.

The U.S. Government is joint author of this work and has the right to use, modify, reproduce, release, perform, display, or disclose the work. PAO case number: AFRL/WS 06-2493; Date cleared: 18 Oct 2006. Paper contains color.

14. ABSTRACT
A shear and stress sensitive film (S3F) is employed on the suction surface of an industry standard low-pressure turbine blade. These tests address the optimization of S3F for low-speed air investigations on a curved surface, and are the first measurements of its kind. S3F provides all three stress components on a surface in a single measurement, and is based on 3D elastic deformations of a polymeric film. New composition films have been developed, and results over a range of Re respective of LPT flow conditions illustrate the need for separate films tailored for the local stress levels in each area.

15. SUBJECT TERMS
Turbine, S3F, skin friction

16. SECURITY CLASSIFICATION OF:			17. LIMITATION OF ABSTRACT:	18. NUMBER OF PAGES	19a. NAME OF RESPONSIBLE PERSON (Monitor)
a. REPORT Unclassified	**b. ABSTRACT** Unclassified	**c. THIS PAGE** Unclassified	SAR	18	Mark McQuilling 19b. TELEPHONE NUMBER *(Include Area Code)* N/A

Standard Form 298 (Rev. 8-98)
Prescribed by ANSI Std. Z39-18

i

Mark McQuilling · Mitch Wolff · Sergey Fonov · Jim Crafton · Rolf Sondergaard

An Experimental Investigation of a Low-Pressure Turbine Blade Suction Surface Using a Shear and Stress Sensitive Film

Abstract A shear and stress sensitive film (S3F) is employed on the suction surface of an industry standard low-pressure turbine blade. These tests address the optimization of S3F for low-speed air investigations on a curved surface, and are the first measurements of its kind. S3F provides all three stress components on a surface in a single measurement, and is based on 3D elastic deformations of a polymeric film. New composition films have been developed, and results over a range of Re respective of LPT flow conditions illustrate the need for separate films tailored for the local stress levels in each area.

Keywords turbine · S3F · skin friction

List of Symbols

c	chord length
C_f	skin friction coefficient
dC_p	change in pressure coefficient, $dC_p = \frac{dP}{q}$
h	film thickness
m	density of air
q	dynamic pressure, $q = 0.5mU^2$
Re	Reynolds number, $Re = \frac{Uc}{v}$
U	characteristic velocity
Greek	
η	dynamic viscosity of oil
μ	modulus of elasticity
v	kinematic viscosity of fluid
ρ	S3F density
τ	shear stress
Subscript	
x	streamwise direction
z	cross-stream direction

M. McQuilling · M. Wolff
Mechanical and Materials Engineering, Wright State University, 3640 Colonel Glenn Hwy, Dayton, OH, 45435
Tel.: 937-255-0633
E-mail: mcquilling.2@wright.edu

S. Fonov · J. Crafton
Innovative Scientific Solutions, Inc., 2766 Indian Ripple Road, Dayton, OH, 45440
E-mail: sfonov@innssi.com

R. Sondergaard
Turbines Branch, Propulsion Directorate, Air Force Research Laboratory, 1950 Fifth St., WPAFB, OH, 45433

1 Introduction

Turbine section designers of modern gas turbine engines continuously strive for increased efficiency and reduced weight. The low-pressure turbine (LPT) section alone can account for up to $1/3$ of the total engine weight (Curtis et al 1997). In the LPT section, the blades are designed for take-off conditions near sea level with high Reynolds numbers (Re). At high-altitude cruise, Re shrinks due to lower air density, allowing a large part of the blade to experience laminar and transitional flow. This low-Re laminar and transitional flow results in an increased susceptibility to separation and transition effects at the higher altitudes. Mayle found that up to 50% of the suction surface can be transitional at any given moment, and this separated and transitional boundary layer decreases blade life and can cause as much as a 2 - 5 point hit in engine efficiency (Mayle 1991). In order to overcome these penalties, designers must accurately understand the flow physics experienced by the LPT section, including the locations of separation onset, transition onset and length, and reattachment if encountered. Only then can they harness the flow in order to recover the losses. In this study, a recently-developed non-intrusive diagnostic technique (S3F) which produces the normal pressure and tangential stresses on a surface is employed to investigate the suction surface flow features of a single Pack-B LPT blade. These initial tests will provide the framework necessary for further study using the S3F technique in evaluating a newly-designed, higher-lift LPT blade in a linear turbine cascade. Higher-lift LPT blades provide the potential to reduce blade counts, which in turn reduces the weight and cost of the gas turbine engine. The S3F technique will provide high-resolution, accu-

rate surface pressure and stress detail required for validation of many CFD codes in use today.

1.1 LPT Studies

Experiments on LPT blades typically consist of 2D cascades of 3 or more blades. Parameters such as free-stream turbulence intensity (FSTI) and *Re* are typically varied in order to match operating conditions encountered in the LPT section of the engine. In his 1993 review of turbomachinery loss mechanisms, Denton suggested the aerodynamic losses sustained in the LPT section can be evenly divided into 3 groups, each accounting for $\frac{1}{3}$ of the total LPT loss: tip leakage loss, endwall loss, and profile loss (Denton 1993). Profile loss can be considered as the entropy generated in the pressure and suction side boundary layers as well as the mixing process after the trailing edge. When separated, the suction side boundary layer and mixing out of the free shear layer (where elevated vorticity is encountered) accounts for the majority of the profile loss. Curtis *et al.* found up to 60% of the total losses were sustained on the suction surface of their LPT blades (Curtis et al 1997).

There are far too many papers on LPT boundary layers and separation research in the open literature to provide a summary here. Classically, focus was concentrated on steady flow environments where time-averaged experimental correlations could suffice for then current design needs. Recently, more attention has been paid to unsteady flow environments where the unsteady mechanisms and secondary flows normally thought to cause loss in the LPT section are taken advantage of to provide reduced aerodynamic losses. Sharma *et al.* found that unsteady effects account for 25-100% of the losses in a steady environment, and can dominate up to $\frac{3}{4}$ of the airfoil from the leading edge (Sharma et al 1990). These complexities include secondary flows generated by the existing turbine row as well as wakes and vortex shedding from upstream blade rows, as depicted in the work of (Wang et al 1997) and (Schobeiri et al 2003) in Figure 1. Both Sharma *et al.* and Wang *et al.* found that the upstream wakes and secondary flows migrate to the suction surface as they travel through downstream blade rows. As CFD techniques advance in more accurately predicting the unsteady environment in the LPT section, turbine designers can tailor their blade geometry to take advantage of upstream disturbances heading their way. Recent studies examining and using the unsteady environment for benefit can be found in (Lou and Hourmouziadis 2000), (Stieger et al 2004), (Houtermans et al 2004), and (Schobeiri et al 2005). The incoming disturbances can effectively force laminar flow into transition either by an inviscid Kelvin-Helmholtz vortex roll-up due to the disturbance penetration into the boundary layer or subsequent turbulent diffusion through the boundary layer (Stieger and Hodson 2004). Either process takes place before the onset of separation or somewhere above the bubble in the free shear layer.

It is interesting to note that wake-induced transition on the suction side of the LPT blade can only occur if the flow is already separated (Howell et al 2002). Using this new understanding of the benefits of an unsteady LPT environment, newer high and ultra-high lift low-pressure turbines have been developed (Howell et al 2001; Bons et al 2005). These high and ultra-high lift LPTs lower blade counts while maintaining efficiency, thus reducing the cost and weight of the engine.

1.2 Skin Friction and Surface Pressure Measurement

Understanding our past capability and limitations with surface force measurements, we'll better understand and appreciate where we're going with new technologies. Probably the first recorded skin friction measurement apparatus was that described by William Froude in 1872, which measured the skin friction experienced by planks dragged across water, as mentioned in recent skin friction reviews (Hakkinen 2004; Plesniak and Peterson 2004). There are basically two types of skin friction sensors: direct and indirect. Direct sensors are advantageous because they do not rely on theoretical or empirical correlations, but can be very delicate and susceptible to system mechanical noise. Indirect skin friction sensors infer the skin friction from other quantities and are typically more robust. Indirect sensors are advantageous because the measured quantity is typically easy to obtain, although the correlation dependence can impose a limit on the applicability range. Surface pressure measurement is classically accomplished by pressure taps or transducers, but only provide information at discrete locations. More advanced techniques such as pressure sensitive paint (PSP) can provide non-intrusive, two-dimensional surface pressure data with significantly less model preparation (Liu and Sullivan 2005).

1.2.1 Global Skin Friction Measurement

Oil film techniques use the proportionality of shear stress with the thinning rate of an oil film according to Equation 1:

$$\tau = \eta \cdot \frac{d}{dt}\left(\frac{dx}{dh}\right) \tag{1}$$

where τ is the skin friction, η is the oil's viscosity, x is the streamwise thinning and h is the thickness of the oil. There are two types of oil film skin friction techniques: interferometric and non-interferometric (Tyler et al 2004). Interferometric oil films work because the oil thickness is less than the coherence length of the light source, and the rays reflected from the thinning oil surface interfere with the rays reflected from the model surface, producing alternating regions of light and dark bands known as "interference fringes" (Plesniak and Peterson 2004). Liu and Sullivan in 1998 used the oil-thickness dependent luminescence of oil seeded with flourescent molecules to determine the oil thickness (Liu and Sullivan 1998). This method eliminates interferometry but requires additional calibration. All oil film skin friction techniques require additional measurement of surface temperature and knowledge of the temperature-oil viscosity relationship (Plesniak and Peterson 2004).
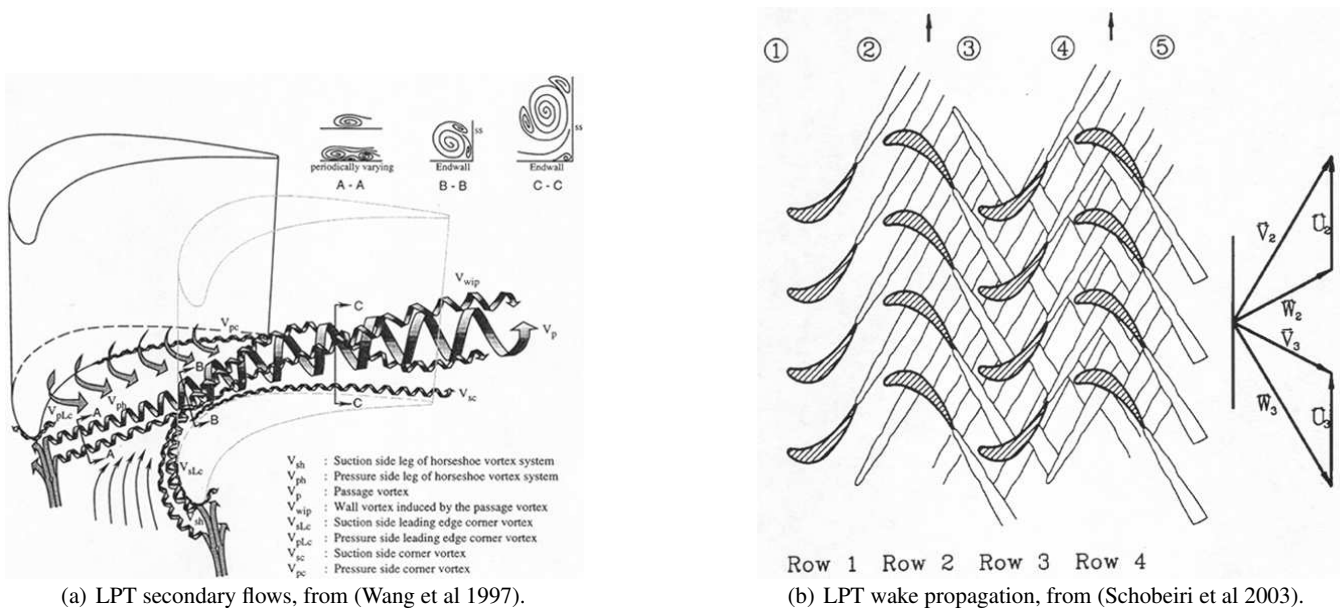
(a) LPT secondary flows, from (Wang et al 1997).

(b) LPT wake propagation, from (Schobeiri et al 2003).

Fig. 1 Examples of complex LPT flow environment.

Another common direct shear sensor which can provide global information are shear-sensitive liquid crystals, which had significant development in the 1960s (Plesniak and Peterson 2004). This technique relies on the change in optical properties of liquid crystals applied to a test surface as they undergo a change in phase. This phase change can be temperature, heat transfer, or shear stress dependent. The optical changes can be temperature, color, or intensity based. Drawbacks using liquid crystals can be the complicated calibration and optical access issues, temperature-sensitivity of liquid crystals, the need to apply a new coat after each test, crystal roughness effects on the flow, and limited availability and cost of the liquid crystals.

Heat transfer analogies which relate the heat transfer obtained with hot-wire or hot-film devices to the skin friction can be used in any fluid where the conductivity of the fluid is greater than the conductivity of the wall (which does not include air) (Plesniak and Peterson 2004). The underlying assumption with these techniques is that the thermal boundary layer lies entirely in the inner region of the velocity profile, which is why the sensors are placed in the viscous sublayer. Advanced probes use multiple-wire hot-wire configurations to provide direction-independent, time-dependent wall shear stress. Another indirect skin friction sensor is an optical sensor which detects the Doppler shift of light scattered from particles passing through divergent fringes in the viscous sublayer. This technique, termed Laser-based or "Fan Fringe" sensors, suffers from the interaction between low data acquisition rates and low seed densities near the wall, and as a result has poor resolution of the sublayer in high Re flows due to turbulent boundary layers.

1.2.2 Global Surface Pressure Measurement

The first global aerodynamic surface pressure measurement was accomplished with pressure sensitive paints (PSPs) in the 1980s (Liu and Sullivan 2005). PSP offers accurate, non-intrusive pressure measurement with increased spatial resolution when compared to conventional taps and pressure transducers. PSP systems use optical techniques to detect the pressure-sensitive luminescence of chromophores suspended in an oxygen permeable binder. As the intensity is a function of the oxygen concentration in the binder, the surface partial pressure of oxygen is related to the luminescent emission. The surface pressure can be obtained from Henry's Law knowing the concentration of oxygen in the main flow. It is generally accepted that PSP techniques for air flow environments must have a velocity greater than ~ 15 m/s for accurate quantitative results.

Liu and Sullivan may have set the stage for S3F development in 1998 when they published their work using luminescent oil films to measure skin friction (Liu and Sullivan 1998). S3F uses the same luminescence technique to obtain film thickness measurements, but additionally provides about 25 times the pressure sensitivity of PSP and comparable S/N with less data averaging, allowing more measurements for a given area in lower dynamic ranges unsuitable for PSP (Fonov et al 2005). S3F also combines a particle tracking algorithm for tracer particles applied on the surface of the luminescent elastic polymer film. The tracer particle translations and film thicknesses (luminescent intensities) are fed into an inverse finite element code which produces the surface normal pressure and tangential surface stress contours that caused the deformations. More information on the S3F technique will be presented in the Experimental Arrangement section. Recently, this technique was

applied to plasma flows in a Mach 5 tunnel at Wright-Patterson Air Force Base in Dayton, OH, alongside temperature- and pressure-sensitive paints (Crafton et al 2005). Since these techniques are optical and require no electrical equipment on the test surface, they are ideal for plasma environments where electrical equipment on the surface would interfere with the plasma kinetics. Information about the science behind or acquisition of PSP, TSP, PIV, or S3F systems can be found on the Innovative Scientific Solutions, Inc. website at www.innssi.com.

1.3 Current Study

The current study seeks to investigate the suction surface flow features associated with a Pack-B LPT blade using S3F. The dynamic range of interest for these initial tests will push the operational envelope of the S3F technique, thus providing a global surface pressure measurement at significantly low flow speed environments which simulate actual LPT flow conditions. Further tests are planned using the S3F technique in a 1-2 m/s flow environment.

2 Experimental Arrangement

All experiments were conducted in the low-speed wind tunnel (LSWT) located at ISSI in Dayton, Ohio. The ISSI LSWT is a low-turbulence, open-circuit wind tunnel. Screens upstream of the test section condition the flow and one wall of the test section is made of clear polycarbonate to allow optical access. Although the test configuration does not allow for flow turning as in proper cascade investigations, the current tests help identify relevant issues which need attention while applying S3F on a curved surface in a low-speed environment.

2.1 Shear and Stress Sensitive Film (S3F)

S3F uses a polymeric film impregnated with luminescent molecules and doped with tracer particles on its surface (Fonov et al 2005). The film is created using a shallow cavity that is filled with the S3F material. After polymerization, the elastic film behaves like an incompressible fluid. Upon application of a force, the film deforms but does not compress. The deformation of the film includes both normal and tangential components. Optical access is required, as the luminescent molecules are excited at one wavelength and emit at another wavelength typically detected by a CCD camera. The intensity of the emission wavelength is proportional to the thickness of the film. Both a "flow-off" and "flow-on" image are required in order to track the surface deformations indicated by the movement of the tracer particles between the two conditions. A ratio between the two conditions also provides a means to cancel out sources of error such as unequal illumination and uneven luminophore dispersion. This ratioing

effectively makes the S3F a differential pressure gauge with tunable dynamic range calibration by modifying the film's modulus of elasticity and Poisson ratio. The normal pressure and tangential surface stresses which caused the three-dimensional deformations are determined from an inverse finite element model, whose inputs are the film thickness-sensitive luminescent intensity and the tracer translations between flow-off and flow-on conditions. S3F was developed in order to measure 2D static pressure on a surface without some of the drawbacks of pressure sensitive paints (PSPs) based on oxygen quenching, such as the need for oxygen in the flow environment and the limited pressure sensitivity, dynamic range, and frequency response.

The origin of the S3F technique began in the early 1990s as a direct method to measure surface shear force (Tarasov and Orlov 1990). This approach consisted of mounting a thin film made of a flexible elastomer of known thickness (h) and shear modulus (μ) onto a model surface. Markers were applied to the film and the model surface and an interference method was used to measure the shear deformation of the film caused by flow. The shearing stress was determined using Hooke's law for shear strain. The main drawback of this method is the fact that gradients of the normal component of force, pressure for aerodynamic flows, can also create a shear-type displacement of the film, and thus the method will work well only in the absence of normal pressure gradients. The S3F technique is therefore sensitive to both skin friction and pressure. The potential to produce a single sensor for the measurement of both quantities was recognized by ISSI and has subsequently been under development.

2.1.1 Operating Principles

Some insight into the operation of the S3F technique can be gained by considering the simplified response of the film to normal and tangential loads. The response to a purely normal load is shown in Figure 2(a). As mentioned above, the film will deform under the normal load but will not compress or yield. The local thickness of the film will be modified by the presence of the load near the point of application, and will return to its original shape upon its removal. Maximum surface displacement is a function of the material properties and the applied normal load. Materials are typically formulated in order to ensure a deflection less than 5% of the total film thickness under maximum anticipated loading, and can be produced to provide less than 1% deflection. The issue of concern is to ensure the film displacement does not introduce flow changes due to the surface deflection. The stressed film thickness is a function of the applied normal force, the original thickness of the film, and its shear modulus, h=f(F_N, h, μ). The film responds to gradients in pressure and not to changes in static pressure. This can be a significant advantage for several reasons. First, the sensor is a differential rather than an absolute gauge and thus can be tuned for applications that require larger or smaller sensitivity. Furthermore, the result is a shear sensor that is insensitive to static pressure changes.
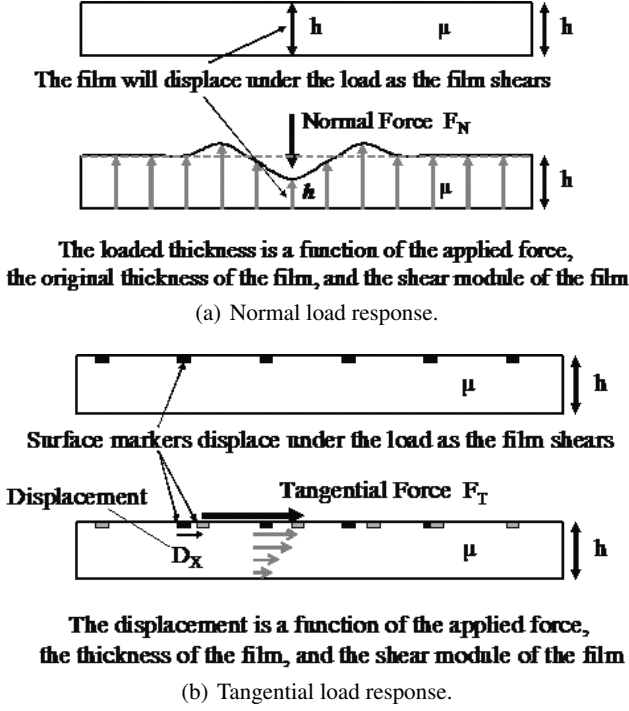
(a) Normal load response.

(b) Tangential load response.

Fig. 2 Simplified S3F responses.

Fig. 3 S3F calibration configuration.

Fig. 4 S3F data acquisition system.

The response of the film to a tangential force is depicted in Figure 2(b). Here, the surface of the film will undergo a tangential displacement due to the load but again will not yield or compress. The response of the film may be visualized by considering a series of markers on the surface of the film. The markers will be displaced as the film shears and this displacement is a function of the film properties. Again, upon removal of the load the film will return to its original shape. The actual response of the film is more complex as the responses are mildly coupled; a pure tangential load will generate a slight change in film thickness and a pure normal load will generate a slight tangential displacement. These simplified examples however demonstrate the basic operation of the S3F.

A final property of interest is the film's frequency response and their potential as a high-frequency probe for both shear stress and pressure. The range of the linear frequency response of such an elastomer is limited by the natural frequency of the shear oscillation, and can be estimated by Equation 2:

$$f_o = \frac{1}{2\pi} \sqrt{\frac{\mu}{\rho h^2}} \qquad (2)$$

where μ is the shear modulus of the film, ρ is the film density, and h is the film thickness. Previous composition variations with $\mu \in$(10 - 1000)Pa and h$\in$(0.1 - 1)mm have produced films with frequency responses from 0.3 to 10kHz.
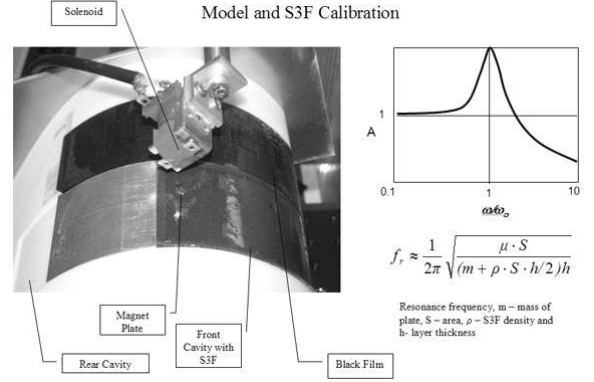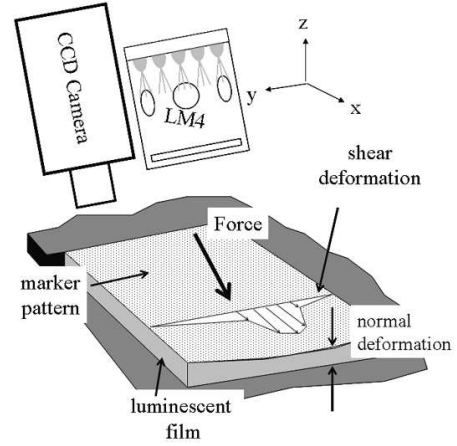
2.1.2 Film Application and Calibration

There are several ways for films to be applied to a surface including spraying with an airbrush, allowing the film to polymerize in a cavity on the model surface, and forming the film in a cavity on a flexible layer which can be glued onto a model surface. Forming films in cavities provides good control of the film thickness and physical properties and control of these parameters is necessary for quantitative measurements of pressure and shear stress. Film formation consists of pouring the polymer components into a flat cavity with a smooth or polished bottom. The film thickness can be estimated by direct measurements using either optical absorption or a capacitive thickness gauge. The film calibration procedure involves applying a specified load to the film surface and measuring the corresponding normal and tangential deformation of the film. For calibrations, the limit of frequency resolution, f_r, is modified from Equation 2 to now include the setup geometry details as shown with the calibration configuration in Figure 3.

2.1.3 S3F Measurement System

The process of measuring pressure and shear is accomplished in two steps. First, the normal and tangential deformation of the film is optically measured. These deformations are then converted to forces using a physical stress/strain model of the film. The experimental setup for this S3F measurement system is presented in Figure 4. All three deformation components can be extracted from a set of flow-off (unloaded) and flow-on (loaded) images taken by a single hi-resolution CCD camera. The normal component in this configuration is measured using the fluorescence signal emitted from a fluorescent probe embedded in the S3F. Two images are acquired, an unloaded and loaded image, and the ratio of these images is a linear function of film thickness. This type of thickness measurement requires a stable light source and at least a 12-bit CCD camera. The tangential displacement is obtained by spatially cross-correlating the flow-off and flow-on images of the surface providing a two-component deformation map. The surface of the film is lightly doped with small particles that adhere to the surface of the film under load, and do not alter the surface roughness characteristics of the film. This combined fluorescence and cross-correlation procedure was selected for the first generation system because it could be implemented using a single CCD camera.

2.1.4 Stress Analysis Model for Force Determination

The process of converting deformations to physical stresses is based on a physical stress analysis model of the film. Consider a 1D load applied to the film surface; in this case the film deformation can be treated in 2D space. A rectangular cavity of specified thickness on a plate is filled with an S3F. Constant loads (normal or tangential) are applied to a small region on the film surface. Since the S3F is an elastic solid, it is deformed under the applied force, and a point in the solid originally at (x,y) is moved to (X,Y) upon application of the load. If the displacement vector $\mathbf{r} = (\mathbf{X} - \mathbf{x}, \mathbf{Y} - \mathbf{y})$ is small, Hooke's Law relates the stress tensor σ inside the solid to the deformation (strain) tensor ε:

$$\sigma_{ij} = \lambda \delta_{ij} \nabla \cdot \mathbf{r} + \gamma \varepsilon_{ij} \tag{3}$$

with

$$\varepsilon_{ij} = \frac{1}{2} \left(\frac{\partial r_i}{\partial x_j} + \frac{\partial r_j}{\partial x_i} \right) \tag{4}$$

where δ_{ij} is the Kronecker delta ($\delta_{ij} = 1$ if $i = j$, $\delta_{ij} = 0$ if $i \neq j$), and λ, γ are the Lame's constants describing the mechanical properties of the material in terms of the modulus of elasticity μ, and Poisson ratio υ:

$$\lambda = \frac{\mu \upsilon}{(1+\upsilon)(1-2\upsilon)}, \gamma = \frac{\mu}{1+2\upsilon} \tag{5}$$

Writing the equation of elasticity in a form for the displacement vector $\mathbf{r}(x)$ in a cavity with volume Ω and zero displacement boundary conditions excluding the contact surface Γ, $\mathbf{r}(x)$ is found for all virtual displacements $\mathbf{w} \in \Omega$ that satisfy:

$$\int_{\Omega} [\mu \varepsilon_{ij}(\mathbf{r}) \varepsilon_{ij}(\mathbf{w}) + \lambda \varepsilon_{ii}(\mathbf{r}) \varepsilon_{jj}(\mathbf{w})] d\Omega = \int_{\Gamma} \tau \cdot \mathbf{w} d\Gamma \tag{6}$$

To further simplify the physical model in Equation 6, the response of the film can be modeled using the response functions of the film to individual normal and tangential loads. The response function of the film to a normal load at the surface, $\delta_{\mathbf{n}}(\mathbf{x})$, includes a normal response function, $\mathbf{n_n}(\mathbf{x})$, and a tangential response function, $\mathbf{n_s}(\mathbf{x})$. Likewise, the response function due to a tangential load, $\delta_{\mathbf{s}}(\mathbf{x})$, includes both a normal, $\mathbf{s_n}(\mathbf{x})$, and tangential, $\mathbf{s_s}(\mathbf{x})$, response function. The elastic reaction, $\mathbf{R}(\mathbf{x}) \equiv (R_x, R_y)$, can be expressed as the convolution of the response matrix and the applied load components. Assuming a linear system, the above formulation yields:

$$\mathbf{R}(\mathbf{x}) = \int \mathbf{G}(\mathbf{x} - \mathbf{x}') \mathbf{L}(\mathbf{x}') \mathbf{dx}' \tag{7}$$

with

$$\mathbf{G}(\mathbf{x}) = \begin{pmatrix} n_n & n_s \\ s_n & s_s \end{pmatrix}$$

and

$$\mathbf{L}(\mathbf{x}) = \begin{pmatrix} L_x \\ L_y \end{pmatrix}$$

where $\mathbf{G}(\mathbf{x})$ is the response matrix and $\mathbf{L}(\mathbf{x})$ are the applied loads. If $\mathbf{G}$ can be determined experimentally or by a Finite Element model, $\mathbf{L}$ can be determined by deconvolution of Equation 7:

$$L = G^{-1} \cdot R \tag{8}$$

Rewriting Equation 7 in a discrete form for the reaction of the film to an arbitrary set of loads applied at discrete surface locations yields:

$$R_{nj} = \Delta x \sum_{k=0}^{N} L_{nk} \tilde{n}_n(x_j - x_k) + L_{gk} \tilde{s}_n(x_j - x_k) \tag{9}$$

$$R_{sj} = \Delta x \sum_{k=0}^{N} L_{nk} \tilde{n}_s(x_j - x_k) + L_{gk} \tilde{s}_s(x_j - x_k) \tag{10}$$

where R_{nj} and R_{sj} are the normal and tangential reactions, respectively, and $L_j = (L_{nj}, L_{sj})$ are the discrete loads applied at surface locations $x_j = [x_o, x_n]$. This system of linear equations with unknown $\mathbf{L_k}$ has the diagonally dominant matrix

$$\mathbf{G_{jk}} = \begin{pmatrix} n_{njk} & s_{njk} \\ n_{sjk} & s_{sjk} \end{pmatrix}$$
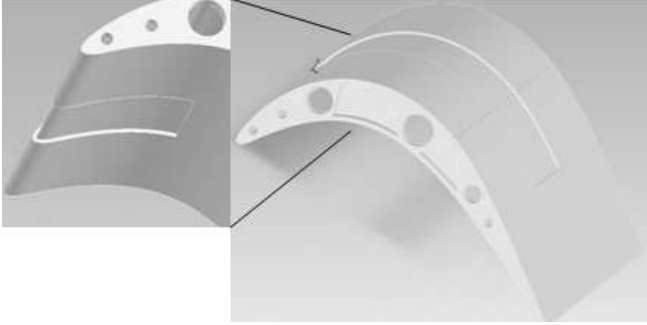
which can be inverted and used to solve for the original loads.
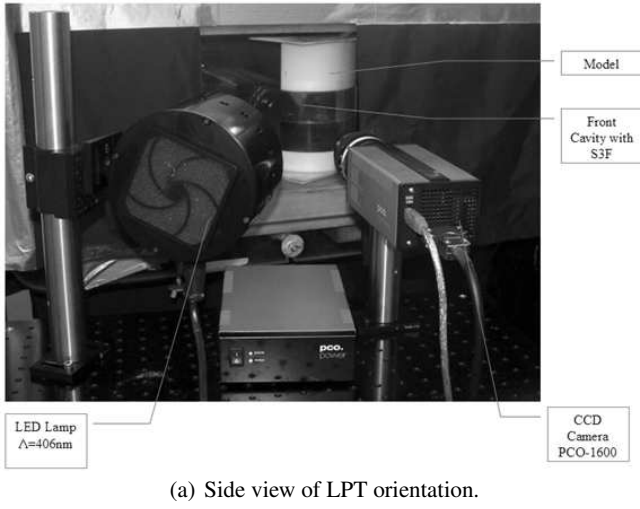
(a) Side view of LPT orientation.
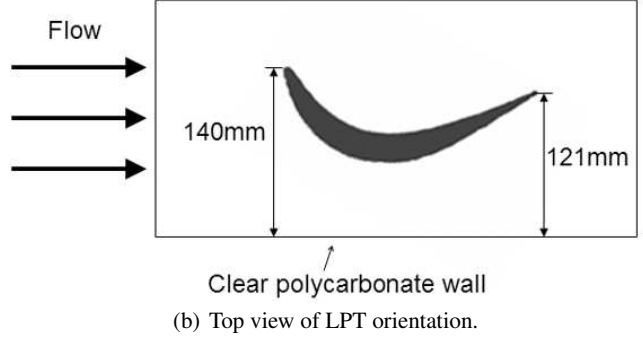
(b) Top view of LPT orientation.

Fig. 6 Pack-B LPT test setup.

Fig. 5 Pack-B LPT with S3F cavity.

2.2 Pack-B LPT

The LPT geometry used herein is the Pack-B profile with a 190.5mm axial chord and 203.2mm span. The blade with its wrap-around 1.5mm deep × 50.8mm wide S3F cavity was made using the rapid-prototyping capability at WPAFB, and is shown in Figure 5.

The orientation of the blade in the straight ISSI LSWT test section did not allow for proper inlet and exit angles typically used for LPT studies. Here it is necessary to remember the goals of this study. First, the current operational envelope of S3F has previously been restricted to water environments or higher speed air environments. These tests will push that envelope by extending the air flow use to very low speeds on the order of 1-7 m/s in order to investigate such phenomena as the low-*Re* lapse in efficiency. Second, issues specific to the LPT geometry, such as the varying gradient levels along the suction surface, were investigated and handled before further testing in realistic LPT orientations. Therefore, all results in this paper are presented with respect to the camera point of view and are only referenced to regions along the suction surface where maximum gradient changes are expected, such as the leading edge and near the locations of maximum curvature. The current orientation of the blade

with S3F inserts and black Mylar strips applied for oil film measurements is shown in Figure 6.

2.3 Data Acquisition

The suction surface of the LPT blade is illuminated with an ISSI LM4 lamp at and detected by a 14-bit PCO.1600 CCD camera with 1600×1200 pixel resolution. A single low-pass filter is used to distinguish the fluorescent emission while an ISSI timing box controls the excitation-detection sequence. Data is collected and stored on a PC.

3 Results

Multi-dimensional skin friction measurement is not a new accomplishment, and as such previous work has developed the proper theory and terminology used to describe such results. Therefore, the terminology as presented in (Tobak and Peake 1982) will be used to aid the description of presented results. The S3F cavity was filled by two separate pieces, one for the leading edge region and one for the trailing edge region (as seen before in Figure 3). Filling the cavity with multiple films instead of one long continuous film was desirable in order to wrap the film around the leading edge and maintain as flush as possible S3F with the blade surface.

3.1 h=1mm, μ=150Pa Film

Results at $U = 13.5$m/s ($Re = 1.83 \cdot 10^6$) for a film thickness of 1mm and shear modulus of 150Pa are presented for the front cavity in Figure 7. A negative spike in streamwise skin friction (τ_x) near the leading edge, indicating surface tension facing upstream, reaches just below -21Pa and is a result of the blade orientation in the straight test section. As
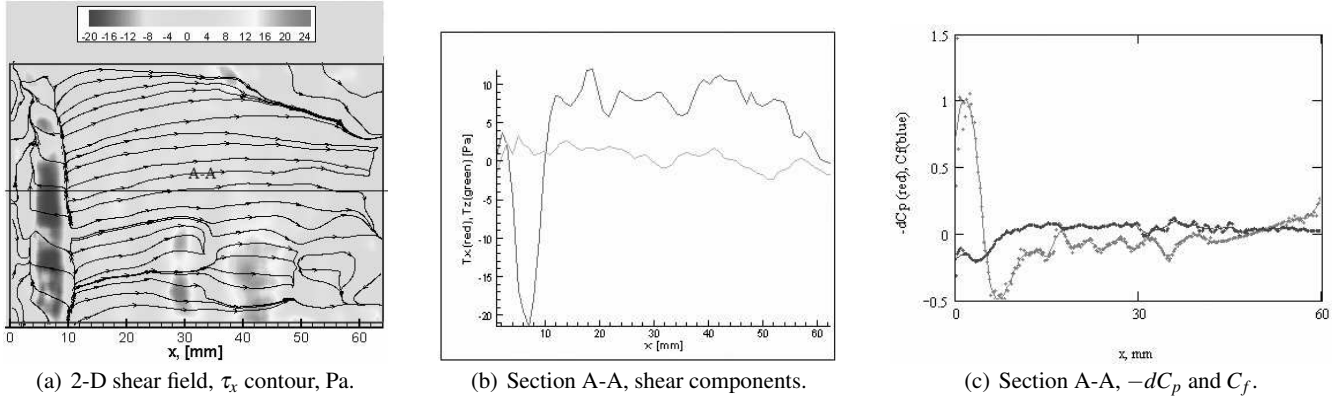
(a) 2-D shear field, τ_x contour, Pa.

(b) Section A-A, shear components.

(c) Section A-A, $-dC_p$ and C_f.

Fig. 7 Front cavity, U=13.5m/s, h=1mm, μ=150Pa.

the oncoming flow is split between the pressure and suction sides near the nodal line of attachment around x=10mm, the flow heading towards the pressure side pulls on the film in the opposite (negative) direction with respect to the suction side. This negative spike region produces a local absolute maximum τ_x-gradient of $\sim$ 6.4Pa/mm. After recovery to positive τ_x, the remainder of the leading edge strip encounters a mean streamwise friction level near 7.5Pa, with local gradients between 0-4Pa/mm. The cross-stream skin friction (τ_z) along section A-A fluctuates around zero, indicating a mostly two-dimensional flow field. The observed 3D influence is believed to be generated by the mounting plates above and below the turbine blade. Waves in the $-dC_p$ plot along Section A-A in Figure 7(c) indicate that the 1mm-150Pa S3F used near the leading edge was too sensitive for a 13.5m/s flow velocity in the current orientation. Further tests will implement an S3F with a better tuned shear modulus for this region.

Results for a similar 1mm-150Pa film in the rear cavity are shown in Figure 8 for 13.5m/s flow velocity. Again a negative spike is noticed around x=30-36mm, but is now due to a surface discontinuity near the upstream edge of the S3F. The rear cavity observes a negative mean τ_x of less than a tenth of a Pascal, indicating a flow separation on the latter part of the suction surface. The streamwise friction gradients in this region are significantly smaller than the front cavity, with absolute values less than 0.04Pa/mm. The cross-stream skin friction τ_z remains in a similar range as τ_x. The difference in skin friction between the front and rear cavities varies by more than an order of magnitude, and illustrates the need for separate S3Fs in each region. The larger mean and gradient levels near the leading edge require a film with smaller sensitivity than the trailing edge. From these preliminary results, the goal was set to develop an S3F with a shear modulus near 30-50 Pa in order to better resolve the expected magnitudes of pressure and shear.

3.2 h=1.5mm, μ=25Pa Film

The next film developed had a shear modulus of 25Pa at a thickness of 1.5mm. Skin friction results for this S3F are presented in Figure 9 for a flow velocity of 7m/s. Here, a focus of separation can be seen in the lower right portion of the plot, indicating a swirling motion of the fluid above. The streamwise shear component for the region of interest encompassed by the box on the left side is shown on the right of the figure in 3-D space. From these tests, the need became clear to apply a black Mylar strip beneath the S3F in order to reduce reflected excitation light and glare from the white material. This reduced the noise collected with the data, but increased the complexity of model setup since the S3F is difficult to glue to the black strip material. The increased noise levels for speeds lower than 7m/s made difficult the second data reduction step of transforming the deformation fields and luminescent intensities into shear and pressure fields. It is expected that future testing will correct the noticed noise issues and will attempt to produce shear and pressure fields in the 1-2 m/s range. In addition, future considerations of construction materials and methods will attempt to replace the white material with a less-reflecting, darker material. It was also found that in order to best resolve the expected flow features it would be necessary to apply the S3F in small 5-10mm wide strips in the flow direction with 1-2mm gaps in between successive strips, running any length along the span. Since the pressure and shear stress gradient levels change so rapidly along the flow direction due to the LPT curvature, the S3F applied in strips would allow different composition and sensitivity S3F pieces to be placed in appropriate regions to better resolve the occurring levels in their respective locations. A sequential series of displacement fields taken at 0.5Hz with the same 1.5mm-25Pa S3F for a flow velocity of 13.5m/s is shown in Figure 10. The x-axis and y-axis are scaled to the pixel distribution of the camera only in order to show the ability of the S3F to track unsteady events. In Figure 10(a), a nodal line of separation appears near x$\approx$ 230, with an accompanying quasi-steady nodal line of attachment near x$\approx$ 1150, indicating the presence of an unsteady separation bubble. Although
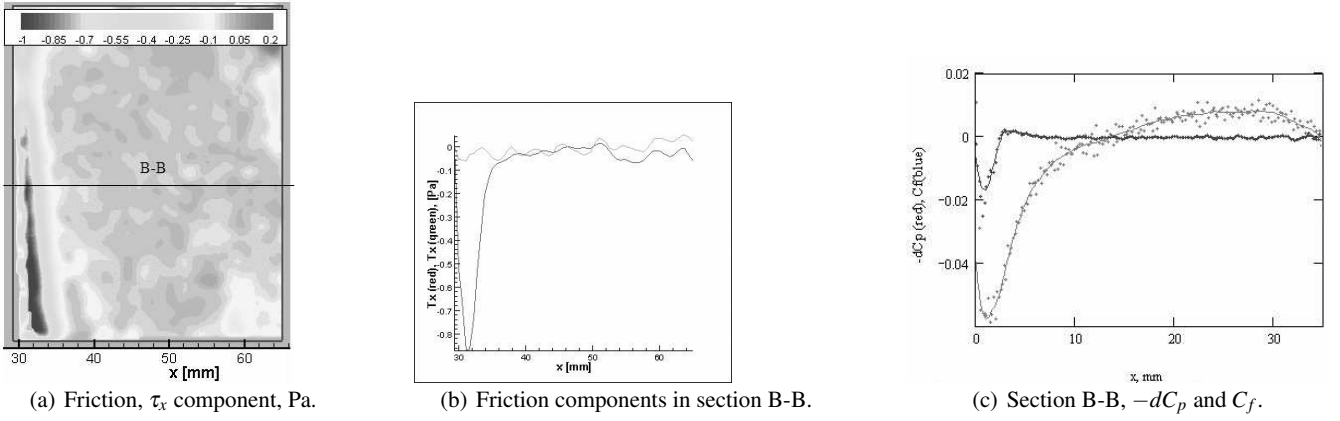
(a) Friction, τ_x component, Pa.

(b) Friction components in section B-B.

(c) Section B-B, $-dC_p$ and C_f.

Fig. 8 Rear cavity, U=13.5m/s, h=1mm, μ=150Pa.

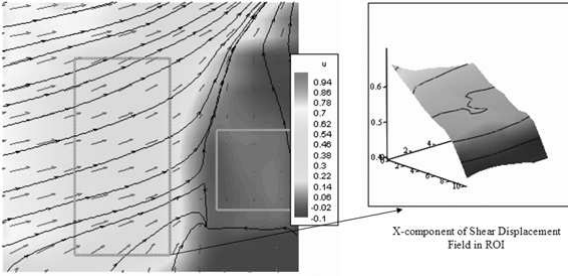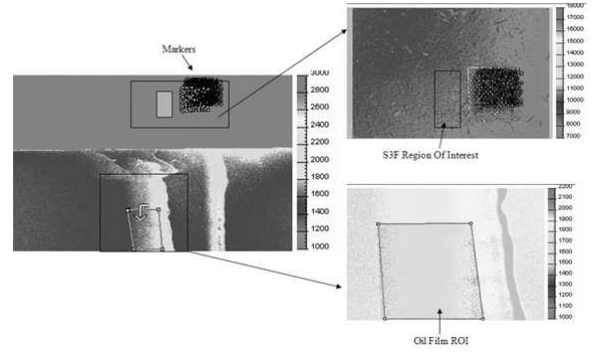**Fig. 9** Shear displacement vectors and streamlines, U=7m/s, h=1.5mm, μ=25Pa.

Fig. 12 S3F-oil film combined measurement regions of interest.

the topological structure remains relatively preserved, the frame capture rate does not exceed the separation frequency and therefore cannot properly resolve the unsteadiness of the event. As mentioned earlier, the upper bound of frequency response for the S3F depends on several factors related by Equation 2.

Displacement fields for $U = 0.7$ to 4.4m/s are presented in Figure 11 for another 1.5mm-25Pa S3F. Evidence of an interaction with the uneven edge of the S3F on the top side of the cavity can be seen here. Similar topological structure can be seen in Figures 11(b) through 11(e), while in Figure 11(f) we see the emergence of a focus of separation near (x,y)=(400,900) and a saddle point of attachment near (x,y)=(700,850), indicating the swirling 3D flow above. The top edge interaction eventually influences a nodal line of separation near x≈ 1150, and a larger separation as the flow velocity approaches 4.4m/s in Figure 11(f), as seen by the upstream directed deformations occurring in the left half of the plot. The attainment of these displacement fields at low speeds, along with oil film verifications, signifies that a proper formulation and implementation of the S3F sensor will be able to produce shear and pressure fields in a flow speed range of 1-7m/s after an adequate amount of noise reduction is accomplished. Additionally, diminishing the region of interest (zooming in) can provide up to 10 times the current sensitivity level used in this paper, providing an-

other means to reduce the noise and increase the S/N ratio for lower speed tests.

3.3 Oil-film Comparison

As mentioned earlier, the lowered signal-to-noise ratio at flow velocities below 7m/s complicated the attainment of shear and pressure fields. Therefore, in order to better trust the small translations indicated in the S3F displacement fields, oil film measurements were made directly below the S3F strip near the front cavity. The combined S3F-oil film setup was presented in Figure 6(a). The regions of interest for combined measurement are shown in Figure 12. For luminescent oil film skin friction measurements, the skin friction is determined by Equation 1. Oil film results showing dx/dh as a function of time for dynamic pressures of 4.6 and 29.6Pa are shown in Figures 13(a) and 13(b). These figures illustrate the linear response of the oil film technique over the dynamic range of interest. The combined S3F-oil film measurements are shown in Figure 13(c), where the S3F measurements are comparable to the oil film results within $\frac{1}{4}$ to $\frac{1}{3}$Pa.
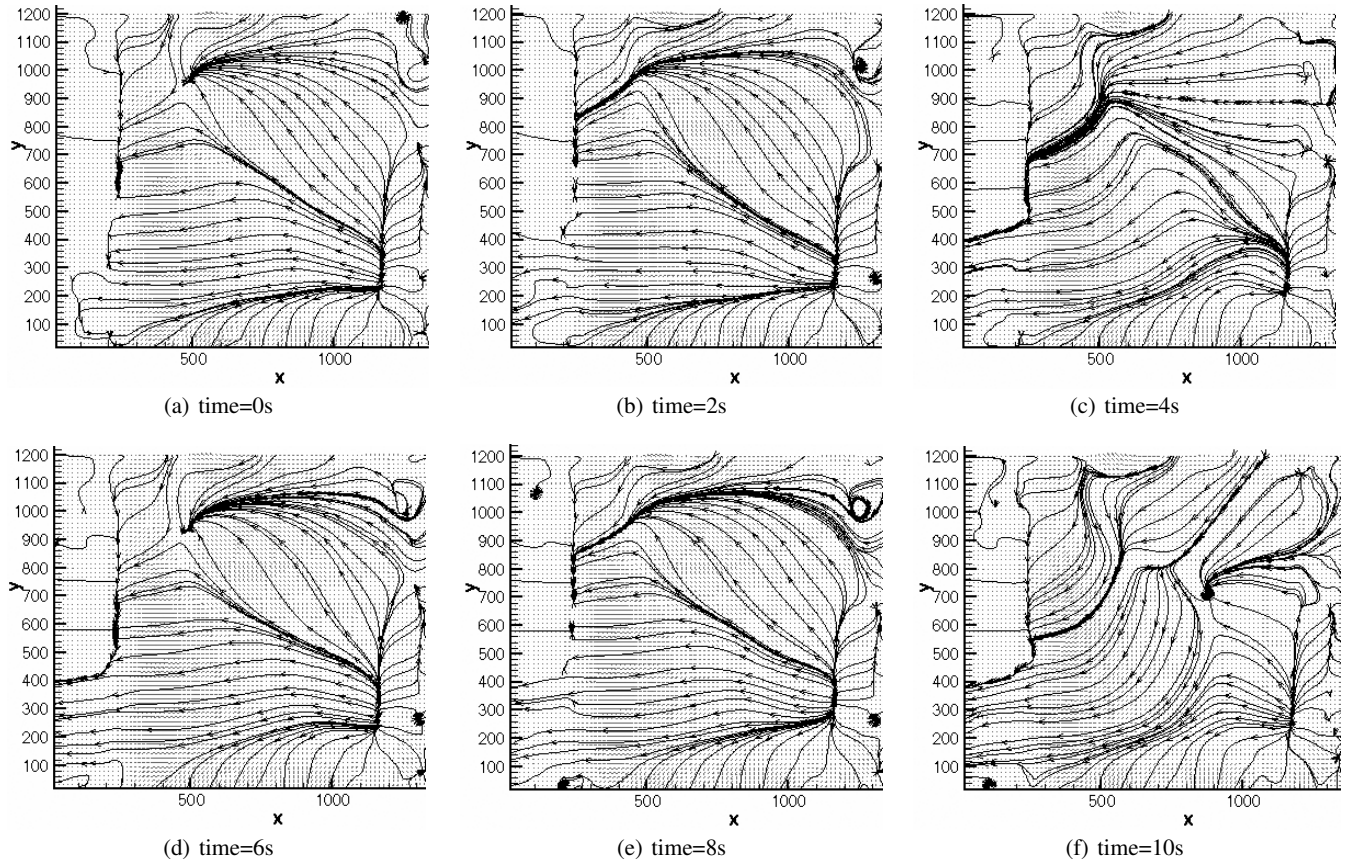
(a) time=0s

(b) time=2s

(c) time=4s

(d) time=6s

(e) time=8s

(f) time=10s

Fig. 10 Sequential series of displacement fields taken at 0.5Hz, U=13.5m/s, h=1.5mm, μ=25Pa.

4 Conclusions

The S3F technique has successfully produced two-dimensional shear fields for flow velocities from 7 to 13.5 m/s on the Pack-B low-pressure turbine blade geometry, corresponding to an Re range of $9.48 \cdot 10^5$ to $1.83 \cdot 10^6$. The goal of applying the S3F technique in a low-speed LPT environment and optimizing geometry related issues has been accomplished in this work. Such LPT-related outcomes include the use of separate, 5-10mm wide strips of S3F along the streamwise direction with 1-2mm gaps instead of long, continuous strips, as well as optimized slot widths, depths, and locations. This optimization is the result of significant differences of over an order of magnitude in the mean shear and up to two orders of magnitude in the shear gradients between the leading and trailing edge regions. These differences require the use of multiple films, as the leading edge region will require a smaller sensitivity S3F than the trailing edge due to the higher levels near the leading edge.

An S3F with a shear modulus of 25Pa and a film thickness of 1.5mm has been successfully used to produce deformation fields at flow velocities from 0.7-4.4m/s, corresponding to an Re range of $8.90 \cdot 10^4$ to $5.97 \cdot 10^5$. In order to accurately resolve shear and pressure fields at these lower speeds below 7m/s, the S/N ratio must be increased above current levels.

5 Future Work

Future tests are planned in order to investigate the suction surface of an LPT cascade of newly-designed high-lift blades using S3F in a 1-2 m/s flow environment. The next tests will focus on increasing the S/N at flow velocities below 7m/s, as well as accomplish the dual validation of a new LPT design and a new transition model by (Praisner and Clark 2004) used in designing the new blades.

References

Bons J, Hansen L, Clark J, Koch P, Sondergaard R (2005) Designing Low-Pressure Turbine Blades with Integrated Flow Control. (ASME Paper No. GT2005-68962)
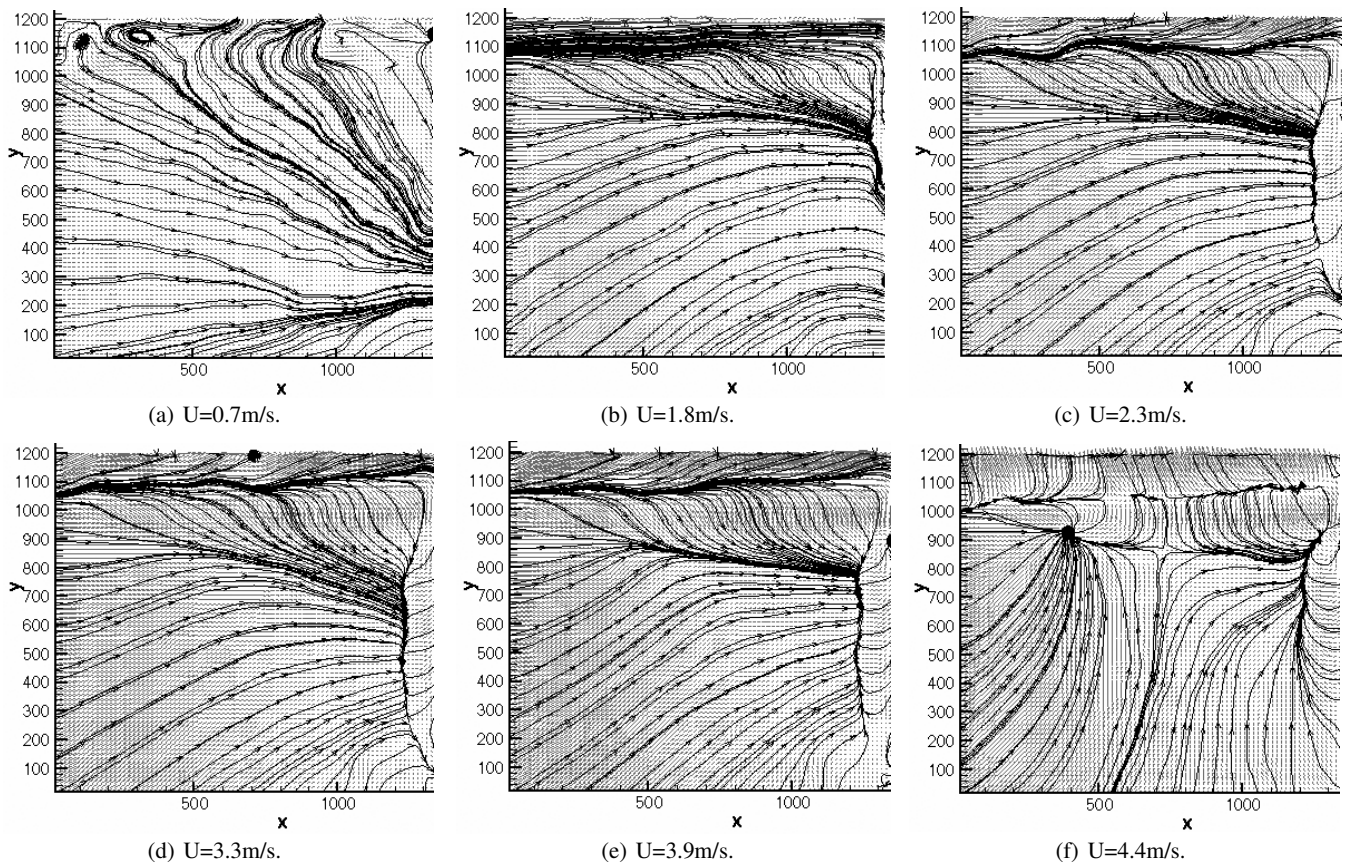
(a) U=0.7m/s.   (b) U=1.8m/s.   (c) U=2.3m/s.

(d) U=3.3m/s.   (e) U=3.9m/s.   (f) U=4.4m/s.

Fig. 11 Displacement fields, h=1.5mm, μ=25Pa.

(a) q=4.6Pa.   (b) q=29.6Pa.   (c) S3F-oil film comparison, h=1.5mm, μ=25Pa.
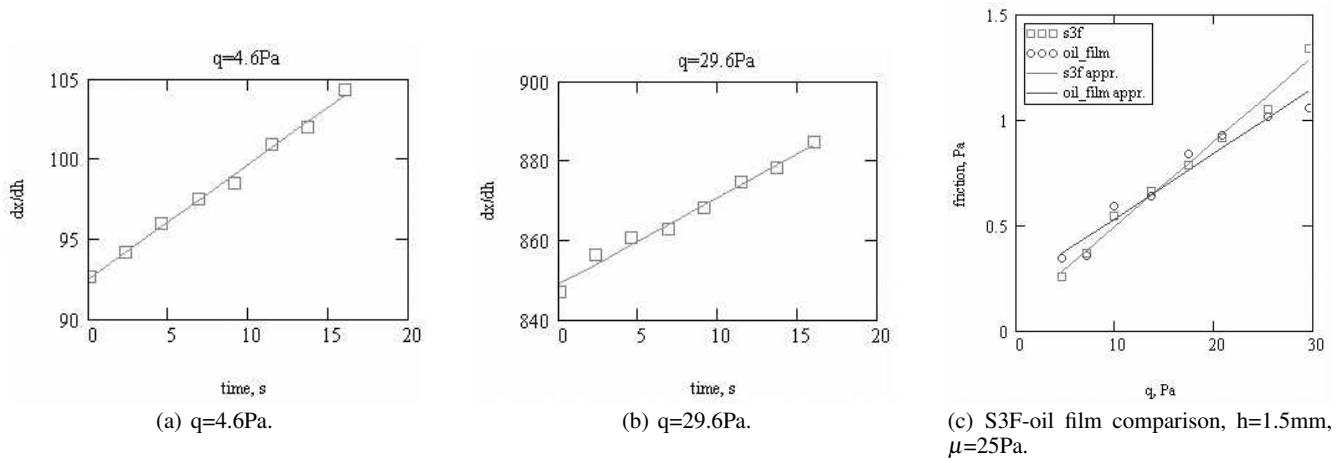
Fig. 13 Oil film measurements.

Crafton J, Fonov S, Jones G, Fonov V (2005) Optical Measurements of Pressure and Shear in a Plasma. (AIAA Paper No. AIAA-2005-5006)

Curtis E, Hodson H, Banieghbal M, Denton J, Howell R, Harvey N (1997) Development of Blade Profiles for Low-Pressure Turbine Applications. J. Turbo.119:531–538

Denton J (1993) Loss Mechanisms in Turbomachines. J. Turbo.115(4):621–656

Fonov S, Goss L, Jones G, Crafton J, Fonov V, Ol M (2005) New Method For Surface Pressure Measurements. (AIAA Paper No. AIAA-2005-1029)

Hakkinen R (2004) Reflections on Fifty Years of Skin Friction Measurement. (AIAA Paper No. AIAA-2004-2111)

Houtermans R, Coton T, Arts T (2004) Aerodynamic Performance of a Very High Lift Low Pressure Turbine Blade With Emphasis on Separation Prediction. J.

Turbo.126:406–413

Howell R, Ramesh O, Hodson H, Harvey N, Schulte V (2001) High Lift and Aft-Loaded Profiles for Low-Pressure Turbines. J. Turbo.123:181–188

Howell R, Hodson H, Schulte V, Stieger R, Schiffer HP, Haselbach F, Harvey N (2002) Boundary Layer Development in the BR710 and BR715 LP Turbines - The Implementation of High-Lift and Ultra-High-Lift Concepts. J. Turbo.124:385–392

Liu T, Sullivan J (1998) Luminescent Oil-Film Skin-Friction Meter. AIAA J 36(8)

Liu T, Sullivan J (2005) Pressure and Temperature Sensitive Paints. Berlin, Germany: Springer-Verlag

Lou W, Hourmouziadis J (2000) Separation Bubbles Under Steady and Periodic-Unsteady Main Flow Conditions. J. Turbo.122:634–643

Mayle R (1991) The Role of Laminar-Turbulent Transition in Gas Turbine Engines. J. Turbo.113:509–537

Plesniak M, Peterson S (2004) Wall Shear Stress Measurements for Conventional Applications and Biomedical Flows (invited). (AIAA Paper No. AIAA-2004-2301)

Praisner T, Clark J (2004) Predicting Transition in Turbomachinery, Part I - A Review and New Model Development. (ASME Paper No. IGTI-2004-54108)

Schobeiri M, Read K, Lewalle J (2003) Effect of Unsteady Wake Passing Frequency on Boundary Layer Transition, Experimental Investigation, and Wavelet Analysis. J Fluids Eng 125:251–266

Schobeiri M, Öztürk B, Ashpis D (2005) On The Physics of Flow Separation Along a Low Pressure Turbine Blade Under Unsteady Flow Conditions. J Fluids Eng 127

Sharma O, Pickett G, Ni R (1990) Assessment of Unsteady Flows in Turbines. (ASME Paper No. 90-GT-150)

Stieger R, Hodson H (2004) The Transition Mechanism of Highly-Loaded Low-Pressure Turbine Blades. J. Turbo.126

Stieger R, Hollis D, Hodson H (2004) Unsteady Surface Pressures Due to Wake-Induced Transition in a Laminar Separation Bubble on a Low-Pressure Cascade. J. Turbo.126:544–550

Tarasov V, Orlov A (1990) Method for determining shear stress on aerodynamic model surface. (Patent of Russia, 4841553/23/1990)

Tobak M, Peake D (1982) Topology of Three-Dimensional Separated Flows. Ann Rev Fluid Mech (14):61–85

Tyler C, Fonov S, Goss L, Crafton J, Jones E, Sarka B (2004) Comparison of Computationally Predicted and Experimentally Measured Skin Friction. (AIAA Paper No. AIAA-2004-2304)

Wang H, Olson S, Goldstein R, Eckert E (1997) Flow Visualization in a Linear Turbine Cascade of High Performance Turbine Blades. J. Turbo.119:1–8